Optical Propagation Through Stratospheric Turbulence

Wilbur P. Brown
Air Force Research Laboratory (AFRL)
Kirtland AFB, NM 87117

Abstract

This paper discusses optical propagation studies performed on the Airborne Laser (ABL) Challenge Project by the Directed-Energy Directorate of AFRL. A separate paper contained in this volume discusses stratospheric turbulence simulations which complement the optical studies reported here. Work performed since the start of FY99 includes: 1) results pertaining to the effect of phase ambiguities and extended reference beacons on adaptive optics system performance; and 2) results used in the design and calibration of scintillometry experiments being performed to determine the strength of atmospheric turbulence on paths of interest to ABL.

Introduction

This paper discusses some results pertaining to optical propagation through stratospheric turbulence obtained from computations performed on the Airborne Laser Challenge project. The Airborne Laser, or ABL, is a boost-phase theater missile defense system which utilizes a directed-energy laser weapon carried on a 747 aircraft. Theater missiles will be detected using plume radiation, tracked using low-power laser illumination and destroyed using a high-power chemical laser. The success of ABL depends on the ability to deliver an adequately stabilized and compensated laser beam on target. The principal challenge is to cope with laser beam distortions introduced on the atmospheric path between the ABL and the target. The Airborne Laser Challenge Project is supporting ABL and the associated technology program by performing computer simulations of pertinent optical, adaptive optical and turbulence phenomenology.

A detailed explanation of the organization of the ABL Challenge Project, the optical, adaptive-optical and stratospheric turbulence phenomenology of interest, and the computational methodology employed to explore these phenomenology is given in a paper published in the 1997 DoD User Group Meeting Proceedings.[1] In the following section a brief summary of the computational methodology is given. This is followed by a discussion of some of the results obtained thus far in FY99.

Computational Methodology

Atmospheric turbulence does not affect the polarization of laser light to a measurable extent. Thus, the propagation of such light is well-described by scalar diffraction theory, as embodied in the Helmholtz equation. Moreover, the scattering produced by atmospheric turbulence is strongly forward-directed at optical wavelengths; and thus, the Helmholtz equation can be solved in the paraxial approximation—which yields a parabolic PDE which can be solved using spectral techniques. The solution is implemented by a split-operator method which divides the propagation into a sequence of two-step processes whereby the field at location z is free-space propagated to z+dz, and then subsequently adjusted to account for the phase shift introduced by the inhomogeneities between z and z+dz. The properties of the atmospheric turbulence are incorporated by generating phase screens having a prescribed spatial spectrum in the plane transverse to the propagation direction. The free-space propagation and phase screen generation are accomplished using a 2-D FFT.

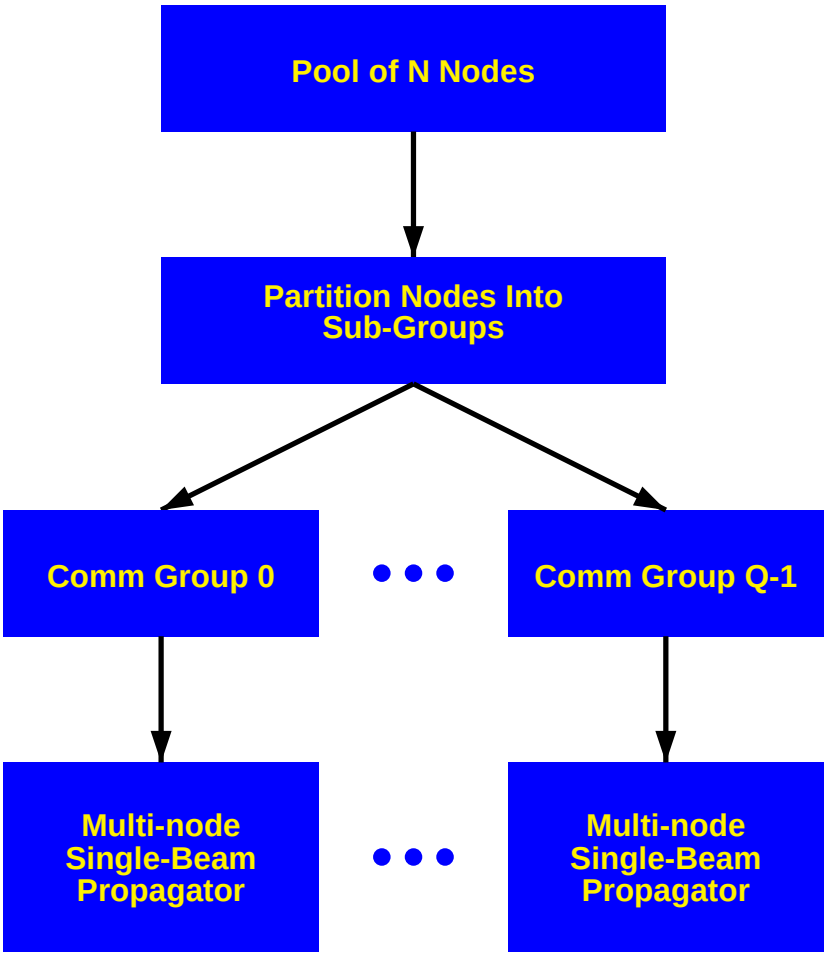

Figure 1. Node partitioning for a multi-beam, multi-node propagator.

To parallelize the propagation code we simply: 1) divide the columns of the field and turbulence phase screen arrays among the processors; and 2) use a parallel 2d FFT to compute the Fourier transforms. This provides an extremely simple and powerful implementation since we can not only propagate one laser using multiple nodes, but can also simultaneous propagate multiple laser beams. This is accomplished by partitioning the nodes into separately identifiable communication groups using the MPI_COMM_SPLIT routine. Each communication group defines a multi-node propagator as illustrated in Figure 1. We use this capability in our simulations of extended target imaging with noncoherent and partially coherent light and in related adaptive optics simulations. For example, in the case of the simulation of the imaging of an extended target illuminated by noncoherent light, we use the fact that a noncoherent image can be approximated by a finite sum of independent coherent speckled images—each image being computed by one of the propagator node groups.

Computational Studies

Some of the results obtained from optical propagation simulation studies performed thus far in FY99 are discussed in this section. This includes: 1) results pertaining to the effect of phase ambiguities and extended reference beacons on adaptive optics system performance; and 2) results used in the design and calibration of scintillometry experiments being performed to determine the strength of atmospheric turbulence on paths of interest to ABL.

Phase Ambiguity and Extended Reference Effects on Adaptive Optics Compensation of Turbulence

Adaptive optics systems typically compensate for the effects of turbulence by sensing the phase of a reference beacon located on or near the object to be imaged or irradiated. It can be shown that if one applies a phase correction equal to the conjugate (negative) of the reference phase the effects of the turbulence will be mitigated. This assumes that the reference is of zero extent and that its phase is faithfully measured and replicated. In practice, these conditions are never totally satisfied. In ABL the target reference is obtained from the field reflected from the target by a laser illuminator beam focused at the target—and thus, the reference, at best, extends over a region comparable to or larger than the diffraction limited width of the illuminator laser target focal spot. In addition to the obvious requirement that the wavefront sensor must have adequate spatial and temporal resolution, the measurement of the reference phase is further complicated by the fact that if the turbulence is sufficiently strong the phase may not be a smoothly varying function of position within the receiver aperture. In particular, if the field has zero amplitude at a point, the phase in the vicinity of that point is ambiguous—i.e., if one traverses a path that surrounds the point and encloses no other zero-points of the field it will be found that the phase does not return to its value at the starting point. Instead, the phase in the vicinity of a field zero exhibits 2π jumps (ambiguities). As described in the following section, this leads to errors in wavefront sensing which degrade system performance.

Least-Squares Wavefront Sensing and the 'Hidden Phase'

Wavefront sensors used in adaptive optics are typically based on the measurement of wavefront slopes—or equivalently phase differences—measured within a set of subapertures. For example, a popular implementation (Hartmann sensor) uses a lenslet array which focuses the light from the lenslet subapertures onto a corresponding array of detectors. If the lenslet subapertures are sufficiently small, the wavefront slopes (phase differences) can be determined from the positions of the focal spots on the detectors. The set of phase differences which span the entire pupil provide a over-determined set of equations which is then solved by a least-squares calculation which minimizes the difference between the measured and computed phase differences. This is referred to as least-squares wavefront sensing. Most wavefront sensors commonly used today are least-squares wavefront sensors—e.g., wavefront sensors based on shearing interferometry also measure wavefront slopes and typically use a least-squares algorithm to determine the corresponding phase values.

The problem with least squares wavefront sensing is that such a sensor does not see the phase ambiguities described above.[2] To provide an understanding of this we note that the phase differences measured by the wavefront sensor can, in general, be described as the sum of two vector components. One of these components is the gradient of a scalar function and the other is the curl of a vector function. When the phase function is smooth and continuous the curl term is zero—and this is the situation which exists when the phase is unambiguous. The curl term describes the additional, non-smooth, phase variation that occurs when ambiguities are present—i.e., when the field goes to zero within the domain of interest. It can be shown that the least-squares solution to the wavefront sensing problem

depends on the divergence of the measured phase difference vector. But the divergence of a vector derivable as the curl of another vector is zero. Thus, a least-squares wavefront sensor does not see the phase associated with the phase ambiguities—and we refer to this phase as the 'hidden phase'.

Implementation of a Generic Least-Square Wavefront Sensor Model For Computational Studies

It can be shown that the phase function ϕ determined by the least-squares formulation of the wavefront sensing problem satisfies the following discrete version of Poisson's equation[3]

$$(\phi_{i+1,j} - 2\phi_{i,j} + \phi_{i-1,j}) + (\phi_{i,j+1} - 2\phi_{i,j} + \phi_{i,j-1}) = \rho_{i,j}\,, \tag{1}$$

$$\rho_{i,j} = (\Delta^x_{i,j} - \Delta^x_{i-1,j}) + (\Delta^y_{i,j} - \Delta^y_{i,j-1})\,, \tag{2}$$

where the Δ's are the measured phase differences. Note that the quantity ρ on the right side of Eq. 1 is the discrete version of the divergence of the phase difference measurements—and thus, does not include the effect of the phase ambiguities, as discussed above. The boundary conditions appropriate for the solution of the least-squares wavefront sensing problem are the Neumann conditions which require that the derivative of the phase function be zero at the boundary.*

We have implemented a solution of Eqs. 1–2 using a discrete Cosine transform. The idealized wavefront sensor used in the computational studies computes phase differences between mesh points by computing the product of the field at a mesh point with the conjugate of the field at an adjacent point and then using the arctangent function to compute the phase difference. Two types of wavefront sensing are modeled depending on the nature of the reference beacon. In the simplest case we model the reference as a coherent 'point source'—approximated by a small Gaussian source. In this case the phase differences are computed and used directly as described above. A more complicated model is used to represent an extended reference beacon. In this case we assume that the beacon radiation is noncoherent. This type of beacon is modeled by computing the phase differences for a set of coherent speckle field realizations of the beacon and then adding the phase difference measurements weighted by the average of the irradiance at the respective field points. The weighting is done to represent the fact that a least-squares wavefront sensor effectively does the same type of weighting in its measurement of the phase differences of a noncoherent source. The speckle realization approach used here is the same as that used in the modeling of noncoherent target imaging. We have found that the addition of 16 speckle realizations provides an adequate simulation of noncoherent wavefront sensing.

Results Pertaining To Phase Ambiguity and Extended Target Referencing Effects.

The simulations were performed for path and optical parameters appropriate to the Airborne Laser Atmospheric Characterization Testbed (ABLACT) experiments. These experiments are being conducted at White Sands Missile Range (WSMR) on a path between North Oscura Peak (NOP) and Salinas Mountain. The path length is approximately 51km, the wavelength is .987μm, and the receiver/transmitter aperture is 70cm. The strength of the turbulence is characterized by the refractive index structure function C_N^2—which was assumed to be constant along the path. Results have been obtained for values of C_N^2 spanning a range from weak to relatively strong turbulence.

To explore the effect of phase ambiguities on wavefront sensing we have considered two idealized cases. In the first case, the adaptive optics reference beacon is a Gaussian beam

* It should be noted that the formulation discussed here applies only to a rectangular geometry.

approximation to a point source. The target-plane irradiance distribution of the Gaussian beam is

$$I(\mathbf{x}) = I_o \exp(-\frac{|\mathbf{x}|^2}{\rho_o^2}) \,, \tag{3}$$

$$\rho_o = d/3 \,, \tag{4}$$

where d is defined such that approximately 90% of the energy is within a circle of diameter d. We thus refer to the Gaussian beam as having a ('effective') diameter d. d was 2cm for the results presented here—which is smaller than the resolving capability of the scoring-beam transmitter aperture and thus should yield adaptive compensation results characteristic of an unresolved point reference. In the second case, the adaptive optics reference is a flat disk which emits noncoherent radiation. The diameter of this disk was varied from 3 to 90cm.

In directed-energy applications the goal of adaptive optics compensation is to restore the ability to focus a transmitted laser beam to a diffraction-limited spot on a distant target immersed in a distorting medium. The degree to which this is achieved is commonly expressed in terms of the Strehl ratio. Results are presented here for two types of Strehl ratio: 1) an on-axis Strehl, which is the ratio of the boresight peak irradiance obtained with adaptive compensation for path distortions to that which is obtained with a diffraction-limited beam propagated through a vacuum; and 2) a bucket Strehl, which is the ratio of the energy contained within a finite aperture (photon bucket) centered on the boresight with adaptive compensation to that obtained in the same aperture for vacuum propagation. These Strehl ratios are indicative of the success in compensating for the effect of extended path distortions on the distribution of the irradiance at the target. For the purpose of assessing the impact of phase ambiguities on wavefront sensing we have computed an additional Strehl ratio which is the ratio of the on-axis peak irradiance that would be obtained if the compensated field reflected from the adaptive optics corrector mirror were were brought to focus in a vacuum to that which would be obtained if all of the phase of the incoming field were sensed and removed by the compensating mirror. This is a 'local' Strehl ratio which is unity when there is no 'hidden phase' and thus it is a measure of how well the wavefront sensor is working.

Results obtained in the point reference studies are shown in Figures 2 and 3. In Figure 2 results are shown for the local on-axis Strehl ratio for the ABLACT/NOP path as a function of the strength of the turbulence. In these simulations we computed the local on-axis Strehl ratio for 200 independent realizations of path turbulence. Note that there is not a unique Strehl ratio for any given strength of turbulence, but rather the Strehl fluctuates randomly within a range that changes as the strength of the turbulence changes. This is caused by the fact that the frequency of occurrence and spatial distribution of phase ambiguities changes as the strength of the turbulence changes. The parameter σ_R^2 is the Rytov theory result for the variance of the natural logarithm of the amplitude of a spherical wave propagated over the path from the target to the adaptive optics receiver[4].

$$\sigma_R^2 = .124 k^{7/6} C_N^2 z^{11/6} \,. \tag{5}$$

σ_R^2 is a measure of the strength of the turbulence effects and these effects vary from relatively weak for $\alpha = .25$ to relatively strong for $\alpha = 2$. Note that the on-axis Strehl is essentially unity for all of the atmospheric realizations when $\alpha = .25$—which implies that very few phase ambiguities exist for turbulence this weak. It is apparent that as the strength of the turbulence is increased, i.e., as α is increased, the frequency of occurrence of phase ambiguities increases.

The results in Figure 3 pertain to the case where we have applied a least-squares phase compensation to a scoring beam propagated back to the target. The Strehl ratios plotted here are computed at the target and results are given for both an on-axis Strehl and a bucket Strehl computed for a bucket that has a diameter equal to $\frac{2\lambda z}{D}$—i.e., a bucket having an extent approximately equal to a diffraction-limited focal spot for a scoring beam having diameter D

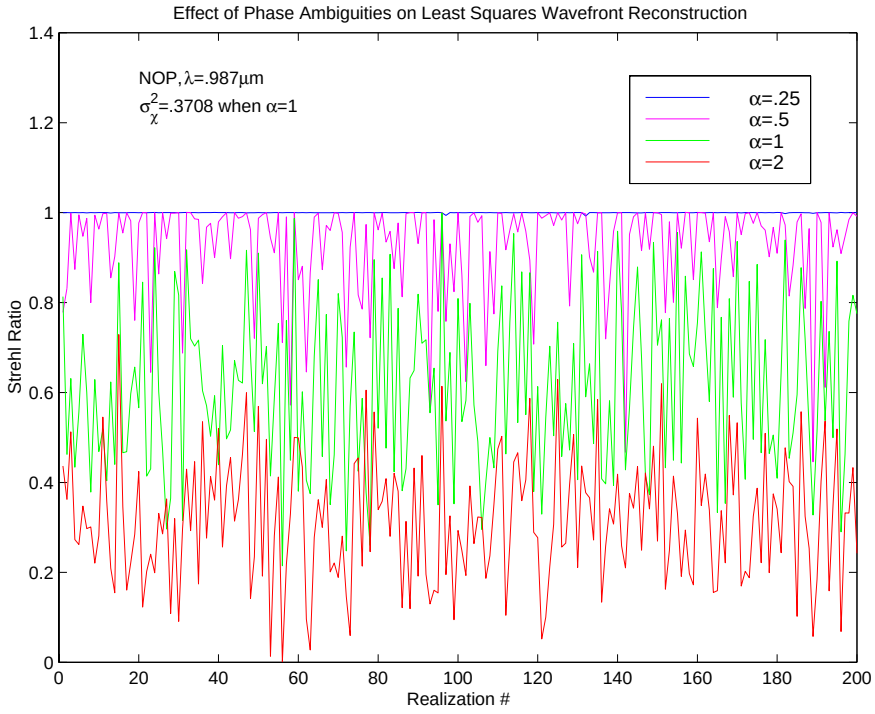

Figure 2. Point-reference, local on-axis Strehl ratio.

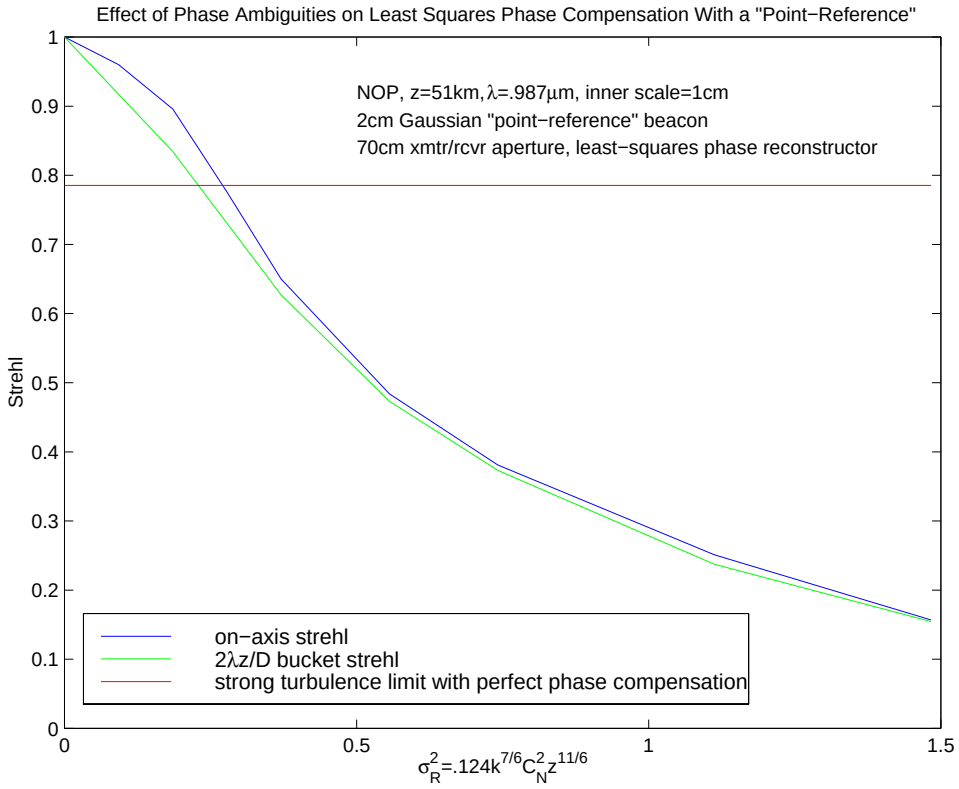

Figure 3. Point-reference, scoring-beam Strehl ratio.

and a target at the distance z. The impact of phase ambiguities is illustrated by the horizontal line which indicates the theoretical value of the on-axis Strehl ratio expected in the limit of very strong turbulence if one could detect and implement perfect phase compensation.*

Results obtained for the case of extended target referencing are shown in Figures 4 and 5. The on-axis Strehl results are given in Figure 4 and the $\frac{2\lambda z}{D}$ bucket results in Figure 5. The Strehl ratios are plotted versus the diameter of the reference disk—where the zero diameter results were obtained using the point source reference described above. If one were to model a coherent extended reference it would be found that the finite extent of the reference significantly affects the fidelity of the phase measurement. For the noncoherent references considered here, however, the effect of reference extent is substantially mitigated by the fact that the wavefront sensor responds essentially to an average over many speckle realizations of the coherent reference—which, as indicated above, we model using the sum of the 16 independent realizations of the speckle field produced by the reference.** For broadband noncoherent radiation this averaging overs over a time interval much shorter than the time for the atmospheric to change. Thus, the averaging eliminates the spurious phase information due to the source extent but does not measurably affect the phase due to the turbulence.

The degree to which a noncoherent extended reference approximates a point source reference is indicated by the Strehl ratio results in Figs. 4 and 5 for the case where the turbulence strength is zero. In this case the degradation in Strehl with increasing disk diameter is due totally to the extended nature of the source. Note that this is a very small effect for the noncoherent reference used in our study. When the turbulence is nonzero, we expect the combined effects of phase ambiguities and anisoplanatism to potentially degrade the adaptive optics performance. In the context used here the term anisoplanatism refers to the decrease in compensation due to the fact that if you focus a scoring beam on the boresight using phase compensation information from a reference displaced from the boresight the phase information will contain errors due to the displacement. Thus, in addition to the degradation in performance due to the presence of phase ambiguities we expect that the performance of an extended target reference will also be affected by these anisoplanatic effects. It is interesting to note that bucket Strehl results are less sensitive to reference size than the on-axis Strehl results. The reasons for this are under study.

Design and Calibration of Scintillometry Experiments.

One of the most important issues in the ABL program is the characterization of the strength and distribution of the stratospheric turbulence likely to be encountered in scenarios of interest. Additionally, in order to interpret the results obtained in the ABLACT experiments being performed at WSMR we must be able to characterize the strength of the turbulence on the NOP path. The measurement of irradiance scintillation (fluctuation) over these paths provides a means of estimating the strength of the turbulence if we know something about its distribution. In order to accurately estimate turbulence strength from

* It should be noted, however, that this result does not tell the entire story for compensation in this limit. It can be shown that as the strength of the turbulence is increased the irradiance in the focal plane has a principal lobe on the boresight which sits on top of a much lower amplitude but wider pedestal of radiation. It is true that as the strength of the turbulence is increased the value of the on-axis peak irradiance stabilizes to the theoretical value given in Figure 3, however, the width of the lobe containing the peak is steadily reduced as the strength of the turbulence is increased. This means that if one were to measure a bucket Strehl instead of the on-axis Strehl it is likely that the diffraction-limited bucket Strehl would be much smaller than the on-axis Strehl in the limit of very strong turbulence.
** Increasing the number of speckle realizations to 32 does not significantly change the results.

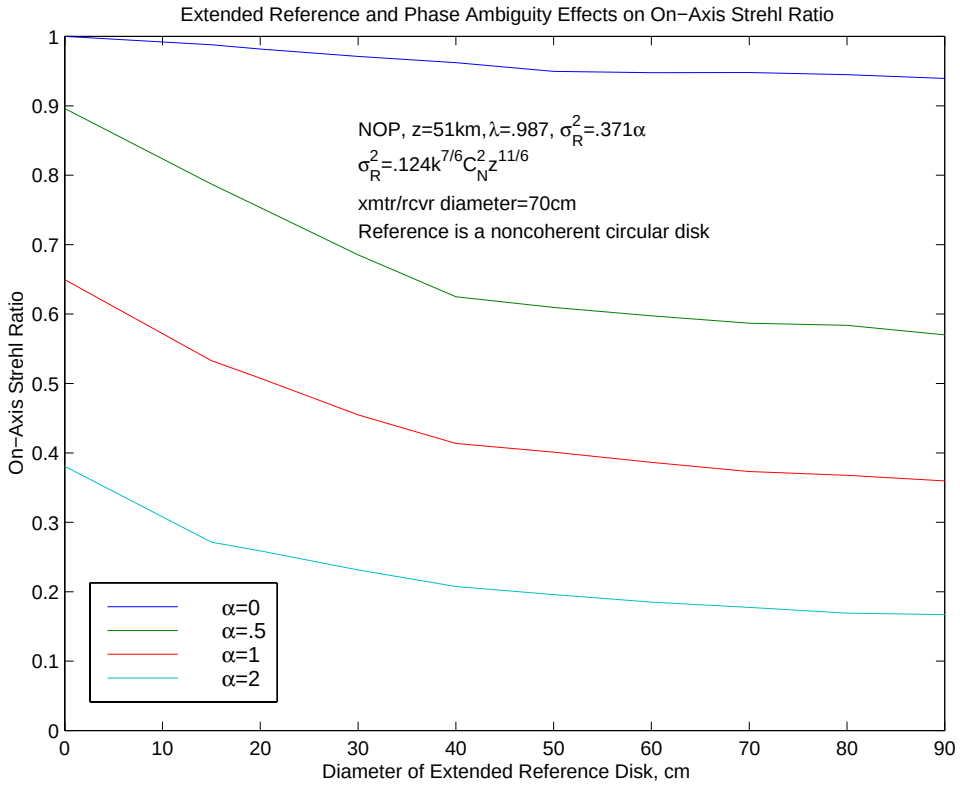

Figure 4. Extended target reference, on-axis Strehl ratio.

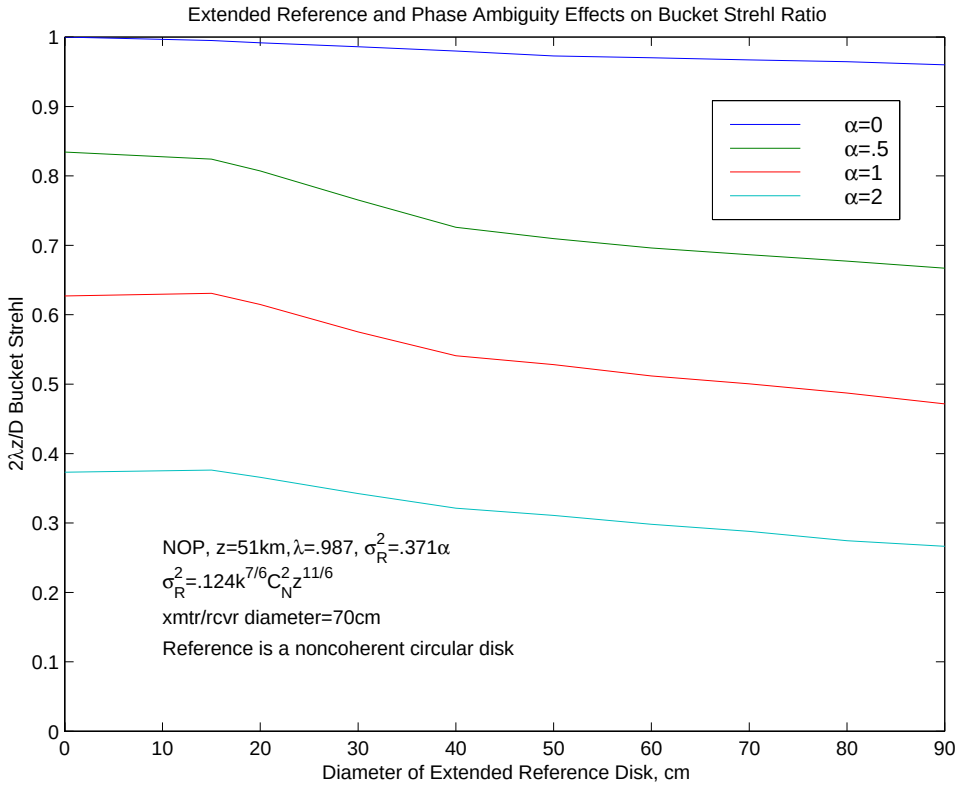

Figure 5. Extended target reference, bucket Strehl ratio.

scintillometry experiments, however, we must account for the fact that the relationship between the measured variance of the irradiance and the strength of the turbulence is nonlinear. We account for this behavior by simulating the propagation on the path of interest. We are currently providing results for the design and calibration of two scintillometry experiments: 1) stellar scintillometry experiments which utilize a KC135 aircraft flying in the vicinity of the tropopause; and 2) scintillometry experiments to be used in the calibration of the ABLACT experiments being performed on the NOP path. This work is described in the following sections.

Design and Calibration of Stellar Scintillometry Experiments

We have calculated the effect of receiver aperture size and detector spectral bandwidth on the measurement of stellar scintillation—assuming that the turbulence is distributed according to the Clear 1 Night model derived from the balloon data, and extended to altitudes above 30km consistent with the decrease in atmospheric density with altitude. Increasing the aperture size and/or the spectral bandwidth of the receiver decreases the magnitude of the measured scintillation and eventually obscures our ability to relate the magnitude of the scintillation to the strength of the turbulence. The sensitivity to these effects depends on the elevation angle of the stellar source. The propagation physics incorporated in the simulation to account for these effects is described in the next section. This is followed by a discussion of the techniques used to relate the simulation results to the stellar scintillation results.

Propagation Physics and Simulation Description

These simulations differ from what we usually have done in the ABL studies in two respects: 1) the stellar light propagates essentially as an extended, plane-wave as it enters the atmosphere, as opposed to the point-source and bounded-beam propagation phenomena we have simulated in the past; and 2) the stellar light has a broad spectral width and thus the effects of wavelength dispersion must be accounted for. The plane-wave propagation is easily accommodated by removing all apodization at the edge of the computational mesh and allowing the initial wave to extend uniformly to the edge of the mesh. Aliasing is not an issue as long as the mesh is sufficiently wide to accommodate the scattering resulting from the turbulent inhomogeneities. In fact, the periodic nature of the FFT solution of the propagation equations ensures that the results mimic plane-wave propagation as long as the above condition is satisfied.* The effects of wavelength dispersion are accounted for by the diffractive nature of the propagation and by explicitly introducing a refractive bending which accounts for the chromatic dispersion in the refractive index. Specifically, we shift the transverse position of successive phase screens to account for the refractive bending associated with the atmospheric density gradient. In calculating the shift, we use the following expression for the wavelength dependence of atmospheric refractive index n

$$(n-1)*10^6 = 64.328 + \frac{29498.1}{(146-1/\lambda^2)} + \frac{255.4}{(41-1/\lambda^2)}\,, \tag{6}$$

where λ is the wavelength in microns. This expression is accurate for all wavelengths of interest in our stellar scintillation studies.

The simulation is performed on a uniform 2048x2048 mesh with 2cm between mesh points. In a typical run 7 to 9 wavelengths are propagated for each of 32 different atmospheric realizations. The irradiance scintillation is measured with an array of detectors dispersed uniformly throughout the mesh. For these studies a 16 by 16 array of detectors spaced 2.56 meters apart is used to compute irradiance statistics. The total number of detector signals

* Scattering which occurs near the edge of the mesh is folded back and reappears at the opposite edge.

available for the statistical calculations is $16 \times 16 \times 32 = 8192$. The effects of finite receiver aperture are calculated by averaging the irradiance over different size apertures, which had diameters of 2, 5, 10 and 15cm in the results presented here.

The effects of finite spectral bandwidth are calculated as follows. For each receiver aperture size we calculate the correlation between the signals at the different wavelengths. We found that the calculated correlations are well fit by a function of the form;

$$f(v) = exp(-a * |v| - b * v^2)\,. \tag{7}$$

where v is the difference in the wavelengths of the light causing the two signals. The constants a and b are determined by a least squares fit of the natural log of the measured correlations to the argument of $f(v)$. The factor RF by which the variance of irradiance scintillation is reduced by a detector having a spectral passband $h(\omega)$ is

$$RF = \frac{\int_{-\infty}^{\infty} d\omega_1 \int_{-\infty}^{\infty} d\omega_2\, h(\omega_1)h(\omega_2) < \delta I(\omega_1)\delta I(\omega_2) >}{< (\delta I)^2 > \int_{-\infty}^{\infty} d\omega_1 \int_{-\infty}^{\infty} d\omega_2\, h(\omega_1)h(\omega_2)}\,, \tag{8}$$

$$< \delta I(\omega_1)\delta I(\omega_2) > = < (\delta I)^2 > f(\omega_1 - \omega_2)\,. \tag{9}$$

In evaluating the reduction factor RF for the stellar scintillometry experiments we have assumed that the spectral passband function can be approximated by a Gaussian of the form

$$h(\omega) = exp(-\frac{\omega^2}{2\lambda_b^2})\,, \tag{10}$$

where the parameter λ_b is related to the full-width, half-max bandwidth $fwhm$ by

$$\lambda_b = \frac{fwhm}{2\ln(2)}\,. \tag{11}$$

Using these relations, we can evaluate the integrals in Eqs. 8 and 9 and obtain the following expression for the reduction factor

$$RF = \frac{\exp(a^2 \widehat{\lambda_b}^{\,2})}{(1 + 4b\lambda_b^2)^{1/2}} \left[1 - \mathrm{erf}(a\widehat{\lambda_b})\right]\,, \tag{12}$$

$$\widehat{\lambda_b}^{\,2} = \frac{\lambda_b^2}{1 + 4b\lambda_b^2}\,. \tag{13}$$

Thus, given the full-width, half-max value of the detector spectral passband and the appropriate values of the parameters a and b determined from the least squares fit of the scintillation data,, we obtain the factor by which the zero bandwidth stellar scintillation is reduced using the reduction factor defined in Eqs. 8–13.

Utilization of Simulation Results in the Estimation of Turbulence Strength From Experimental Data

Experimental measurements of stellar scintillation are characterized by five parameters: 1) the strength and distribution of the turbulence; 2) the altitude of the aircraft; 3) the elevation angle of the path along which the star is observed; 4) the diameter of the receiver aperture; and 5) the spectral passband of the receiver detection system. The approach that we have used to estimate the turbulence strength associated with the experimental measurements is to establish databases of propagation results applying to a wide variety of propagation conditions coupled with the development of a Matlab interpolation routine which is used to interpolate the simulation results to the parameter values pertinent to

the experiment. The initial set of airborne scintillometry experiments were performed in June 1998 using a receiver with a spectral passband centered at .8μm. The database that we computed for those experiments contains results for: 1) turbulence profiles having a strengths of .25, .5, 1, 2, 2.8284, 4, 5.65685, 8, 11.3137 and 16 times the Clear 1 Night model; 2) aircraft altitudes of 12.6 and 14.4km; 3) elevation angles of 6, 8, 10, 12, 14, 16 and 18 degrees; 4) receiver diameters of 2, 5, 7, and 10cm; and 5) spectral passbands of 0, 12, 25, 40, 65, and 100nm. The receiver diameters and spectral passbands are those used in the experimental measurements, and thus, no interpolation is required for these parameters. The Matlab routine first interpolates the database to obtain results pertinent to the aircraft altitude. It then interpolates the resulting database to obtain data pertinent to the elevation angle for that measurement. At this point we have a set of irradiance variance versus turbulence strength values pertinent to the aircraft altitude, receiver diameter, spectral bandwidth and elevation angle of the measured irradiance variance. We then use interpolation to find the turbulence strength associated with the measured variance. In doing this we verify that the interpolation is unique—i.e., we verify that the we are not in a region where the scintillation has saturated and the results are thereby ambiguous. The experiment was designed such that we would seldom be in a saturated condition—principally by excluding elevation angles less than 6 degrees. This is illustrated by the irradiance variance versus turbulence strength results shown in Figure 6. These results were computed for an altitude of 12.6km, a receiver aperture diameter of 5cm and a spectral passband of 12nm. Note that for turbulence strengths less than 8 times the Clear 1 Night value the irradiance variance curves show little evidence of saturation and the determination of the strength from the measured irradiance variance is unique.

The success of the initial set of airborne scintillometry measurements was, at least in part, responsible for the decision to proceed with the development of the ABL system made in the summer of 1998. It was recognized at that time that additional measurements at lower elevation angles would be worthwhile and we are now planning a new set of measurements to be performed in June 1999. In order to reduce the effects of irradiance saturation at lower elevation angles these experiments will be performed with a receiver having a spectral passband centered at 2.3μm. An example of the irradiance saturation characteristics computed for the new experiment is shown in Figure 7.

Calibration of ABLACT Experiments Using Scintillometry

The ABLACT experiments are exploring a number of fundamental adaptive optics and tracking issues of importance to ABL. As indicated earlier, these experiments are being performed on a path between North Oscura Peak (NOP) and Salinas mountain at WSMR. In order to properly interpret the results of these experiments it is important that we have a measure of the strength of the turbulence on this path. This will be done using measurements of the irradiance scintillation of a spherical wave source propagated from Salinas mountain to NOP. The concept of the measurement is similar to that used in the design of the stellar scintillometer experiments but differs in that we hope to unambiguously measure turbulence strengths well into the saturation regime. Based on computer simulation results for irradiance scintillation on the NOP path we believe that we can do this utilizing receivers having different size apertures. The results in Figures 8 and 9 illustrate the basis of this concept. Figure 8 shows the variance of irradiance as a function of turbulence strength for receiver apertures of 1 and 4cm. The finite spatial correlation of the irradiance scintillation results in a reduction in the measured irradiance variance for the larger of the two apertures. Figure 9 shows the ratio of the irradiance variance measured with 1 and 4cm apertures. Note that this ratio is a monotonically increasing function of turbulence strength. We believe that this will allow us to estimate C_N^2 in these experiments well into the saturation regime—a conclusion that could not have be reached without the aid of computer simulation.

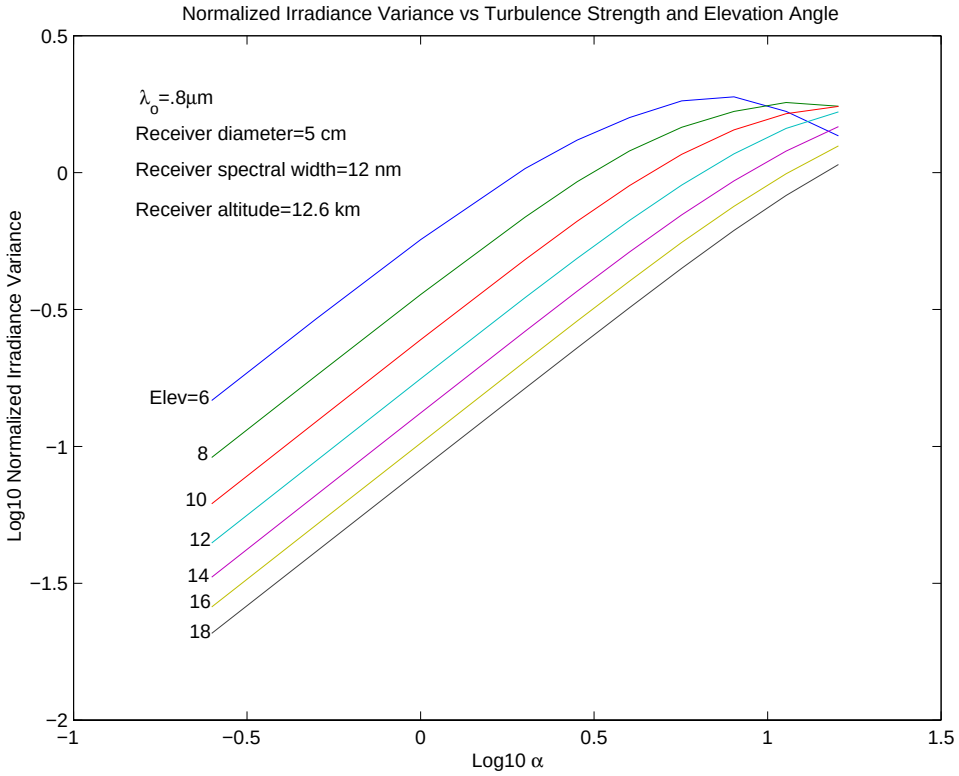

Figure 6. Stellar scintillometry irradiance variance for a receiver with a spectral passband centered at .8μm.

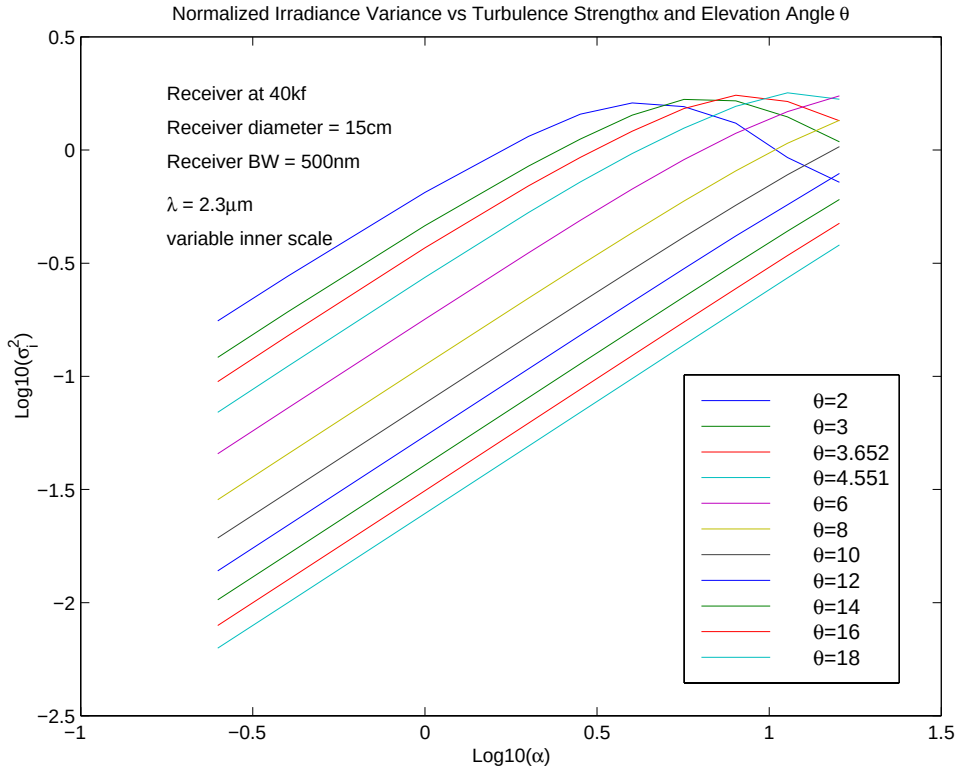

Figure 7. Stellar scintillometry irradiance variance for a receiver with a spectral passband centered at 2.3μm.

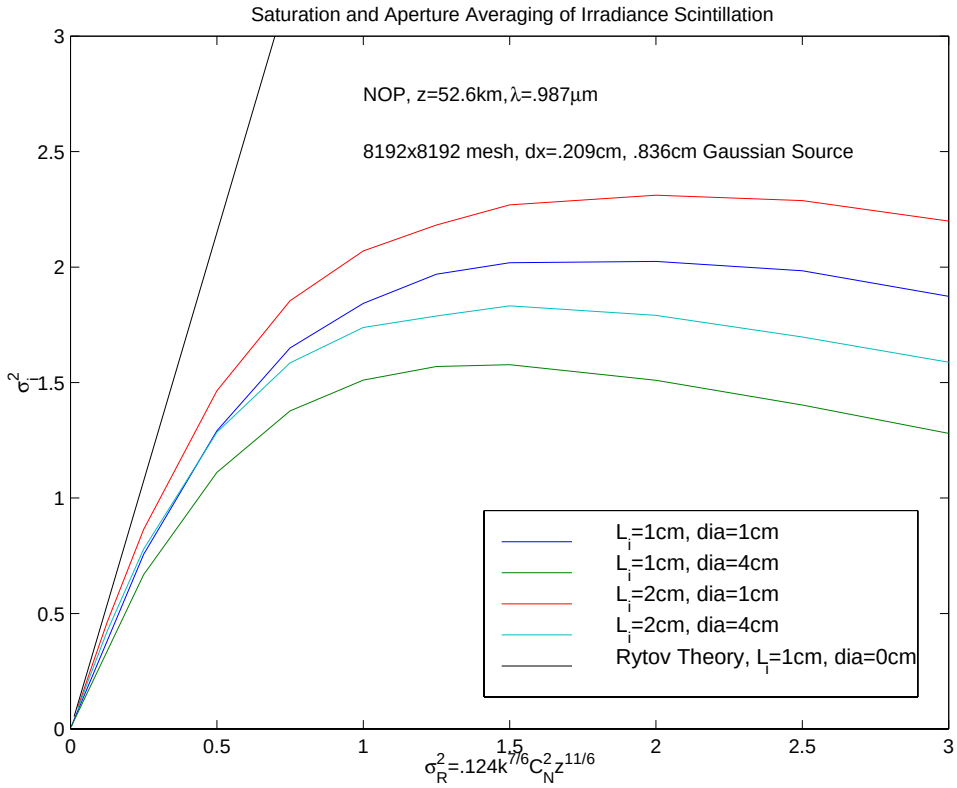

Figure 8. Irradiance variance for the NOP path.

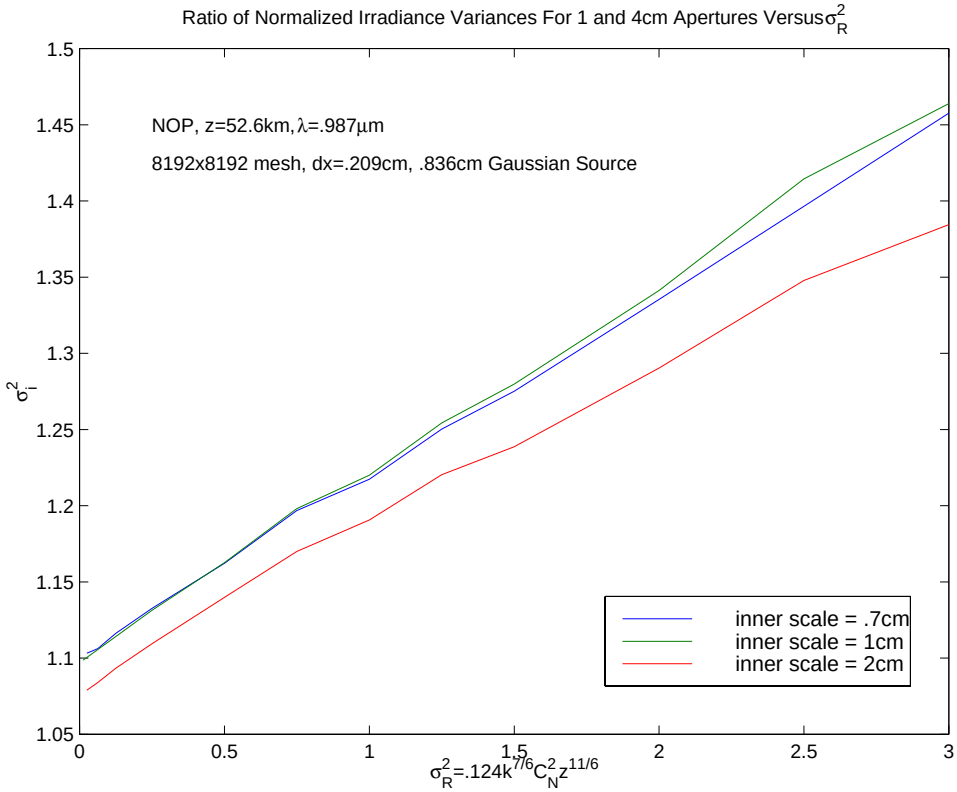

Figure 9. Ratio of irradiance variances for 1 and 4cm receiver apertures.

Acknowledgments

These simulations were performed on the IBM P2SC nodes at the Maui High Performance Computing Center (MHPCC). Technical assistance provided by George Gusciora and Tim Fahey of MHPCC is appreciated. Computer allocations were provided by the DoD Challenge Program managed by the High Performance Computing Modernization Office.

References

1 Wilbur P. Brown, "Airborne Laser", 7th DoD HPC User Group Conference, LaJolla, CA 1997.
2 David L. Fried, "Branch point problem in adaptive optics", J. Opt. Soc. Am. A, **15**, pp 2759–2768, (1998).
3 Dennis C. Ghiglia and Mark D. Pritt, *Two-Dimensional Phase Unwrapping*, pp 186-189, John Wiley & Sons (1998).
4 A. Ishimaru, *Wave Propagation and Scattering in Random Media*, Academic Press (1978).

Figure Captions

1 Node partitioning for a multi-beam, multi-node propagator.
2 Point-reference, local on-axis Strehl ratio.
3 Point-reference, scoring-beam Strehl ratio.
4 Extended target reference, on-axis Strehl ratio.
5 Extended target reference, bucket Strehl ratio.
6 Stellar scintillometry irradiance variance for a receiver with a spectral passband centered at .8μm.
7 Stellar scintillometry irradiance variance for a receiver with a spectral passband centered at 2.3μm.
8 Irradiance variance for the NOP path.
9 Ratio of irradiance variances for 1 and 4cm receiver apertures.